Vibrational mode and collision energy effects on reaction of H_2CO^+ with CO_2†

Jianbo Liu, Brady W. Uselman, Brian Van Devener and Scott L. Anderson*

Received 28th July 2006, Accepted 25th August 2006
First published as an Advance Article on the web 11th September 2006
DOI: 10.1039/b610814h

The effects of collision energy (E_{col}) and five different modes of H_2CO^+ vibration on the title reaction have been studied over the center-of-mass E_{col} range from 0.1 to 3.2 eV, including measurements of product ion recoil velocity distributions. Electronic structure and Rice–Ramsperger–Kassel–Marcus calculations were used to examine properties of various complexes and transition states that might be important along the reaction coordinate. Two product channels are observed, corresponding to Hydrogen Transfer (HT) and Proton Transfer (PT). Both channels are endothermic with similar onset energies of ~0.9 eV; however, HT dominates over the entire E_{col} range and accounts for 70–85% of the total reaction cross section. Both HT and PT occur by direct mechanisms over the entire E_{col} range, and have similar dependence on reactant vibrational and collision energy. Despite these similarities, and the fact that the two channels are nearly isoenergetic and differ only in which product moiety carries the charge, their dynamics appear quite different. PT occurs primarily in large impact parameter stripping collisions, where most of the available energy is partitioned to product recoil. HT, in contrast, results in internally hot products with little recoil energy and a more forward–backward symmetric product velocity distribution. Vibration is found to affect the reaction differently in different collision energy regimes. The appearance thresholds are found to depend only on total energy, *i.e.*, all modes of vibration are equivalent to E_{col}. With increasing E_{col}, vibrational energy becomes increasingly effective, relative to E_{col}, at driving reaction. For HT, this transition occurs just above threshold, while for PT it begins at roughly twice the threshold energy.

I. Introduction

We report a study of the effects of collision energy (E_{col}) and H_2CO^+ vibrational excitation on the reaction of H_2CO^+ + CO_2. The only previous study we are aware of is a Selected Ion Flow Tube (SIFT) study by Adams *et al.*,[1] where no reaction was observed because of significant endoergicity. In this paper, integral cross sections and product velocity distributions were measured for reaction of mode-selectively excited H_2CO^+ with CO_2 over the center-of-mass collision energy (E_{col}) range from 0.1 to 3.2 eV. Two product channels are observed, corresponding to Proton Transfer (PT) and Hydrogen Transfer (HT). An interesting point is that these two channels differ only in which moiety carries the charge, *i.e.*, HCO + $OCOH^+$ (HT) *versus* HCO^+ + OCOH (PT). Furthermore, the onset energies of the two channels are found to be nearly identical, raising the question of what factors should control the product branching. In a statistical picture, one might expect branching to be controlled by the number of accessible rovibrational states associated with each product channel. In cases where the product channels have very different equilibrium structure, one might expect that the channel with the most reactant-like geometry might dominate. In this system, neither factor appears to be important, and branching appears to be controlled by dynamics.

The effects of collision energy on driving endoergic reactions have been studied extensively—indeed, studying the near-threshold E_{col} dependence of reaction cross sections is an important source of information on bond energies and reaction energetics, and behavior at high E_{col} provides insight into reaction dynamics. Less is known about the effects of vibration, particularly for polyatomics, where the relation between the mode excited and the reaction coordinate may be obscure. In fitting the threshold behavior of cross sections to extract energetics, it is commonly assumed that all forms of energy are equivalent.[2,3] Indeed, for some systems that assumption is found to be correct,[4,5] but there are also systems where vibrational excitation is found to be more[6] or less[7] effective than E_{col} at driving reaction near threshold. Well above threshold, collision energy effects tend to saturate, *i.e.*, further increases in E_{col} are ineffective at driving reaction, or may even inhibit reaction by driving competing dissociative channels. In this energy range, vibrational effects on reactivity and product branching often remain large, demonstrating that the form of energy added to a system is important. The nature of the effects, particularly if the effects are strongly mode-specific, provide insight into what types of molecular motions and distortions enhance or inhibit specific bond rupture/formation or isomerization processes.[8,9]

Department of Chemistry, University of Utah, 315 S 1400 E, Room 2020, Salt Lake City, UT 84112. E-mail: anderson@chem.utah.edu
† The HTML version of this article has been enhanced with additional colour images.

II. Experimental and computational details

The guided ion beam tandem mass spectrometer used in this study has been described previously,[4,10–12] along with the operation, calibration and data analysis procedures. The H_2CO precursor was generated from paraformaldehyde (Aldrich 95%) mixed with anhydrous $MgSO_4$ (Merck) at 60 °C.[13] The resulting H_2CO was carried into a pulsed molecular beam valve using a flow of helium at ~1 atm, giving a H_2CO concentration of ~5%.[14] H_2CO^+ can be generated in selected vibrational states with high purity by REMPI through the $^1A_2(3p_x)$ Rydberg state.[15] For this study, H_2CO^+ was generated in its ground state, or with one quantum in the following vibrational modes: ν_2^+ (CO stretch, 0.208 eV), ν_3^+ (CH_2 scissors, 0.143 eV), ν_4^+ (CH_2 out-of-plane bend, 0.114 eV), ν_5^+ (CH_2 asymmetric stretch, 0.337 eV), and ν_6^+ (CH_2 rock, 0.101 eV). The ions were generated inside a short radio frequency (rf) quadrupole ion guide that focused the ions through a pair of ion lenses into a quadrupole mass filter. Mass-selected ions were collected and collimated by a lens set equipped with variable apertures, and a electrode pair used to time-gate the ion pulse. The combination of controlled collection radius and time-gating allows production of a mass-selected beam with narrow kinetic energy spread ($\Delta E \approx$ 0.1 eV).

The mass-, vibrational state-, and kinetic energy-selected primary beam was injected into a system of 8-pole rf ion guides.[16] In the first segment of the guide, ions were passed through a 10 cm long scattering cell containing CO_2 at 1×10^{-4} Torr. CO_2 (Matheson, 99%) was used without further purification. Product ions and unreacted primary ions were collected by the ion guide, passed into a second, longer guide segment for Time-Of-Flight (TOF) analysis, then mass analyzed and counted. Integral cross sections were calculated from the ratio of reactant and product ion intensities, and the calibrated target gas pressure · length product. TOF was used to measure the reactant ion beam velocity distribution (and thus the E_{col} distribution) at each nominal E_{col}, and also to measure the product ion axial velocity distributions discussed below.

For each reactant state, we cycled through the series of E_{col} values several times in order to minimize systematic error from drifting potentials, *etc*. Each cycle includes measurements both with the CO_2 target gas flowing into the scattering cell, and with the identical flow directed into the surrounding vacuum chamber, allowing subtraction of signal from reactions occurring outside the cell. As a check on reproducibility, we measured the cross sections for the ground state, both at the beginning and end of each complete experimental run. Finally, the entire set of experiments was repeated several times. Based on the reproducibility of the cross section measurements, the relative error (*e.g.*, uncertainty in comparing data for different vibrational states or E_{col}) is about 10% (see error bars on Fig. 5). The uncertainty in the absolute scale of the cross section is also estimated to be ~10%, primarily resulting from uncertainties in target pressure and collection efficiency for slow product ions.

To map out the reaction coordinate, electronic structure calculations were performed at the B3LYP/6-311++G** level of theory, using GAUSSIAN03.[17] Geometries were optimized by calculating the force constants at every step. The vibrational frequencies and zero-point energies were scaled by a factor of 0.9613 and 0.9804, respectively.[18] Transition States (TSs) were verified to be first-order saddle points by frequency calculations. For the reactants and all observed product species, we also performed calculations at the G3 level of theory. Rice–Ramsperger–Kassel–Marcus (RRKM) rate and density of states calculations were done with the program of Zhu and Hase,[19] using its direct state count option, and frequencies and energetics from the B3LYP/6-311++G** calculations.

III. Results and analysis

A. Integral cross sections

The integral cross sections for reaction of CO_2 with H_2CO^+ in various initially selected states, are shown in Fig. 1. To allow comparison of the effects of E_{col} and vibrational energy (E_{vib}), the data are plotted against $E_{total} = E_{col} + E_{vib}$. The

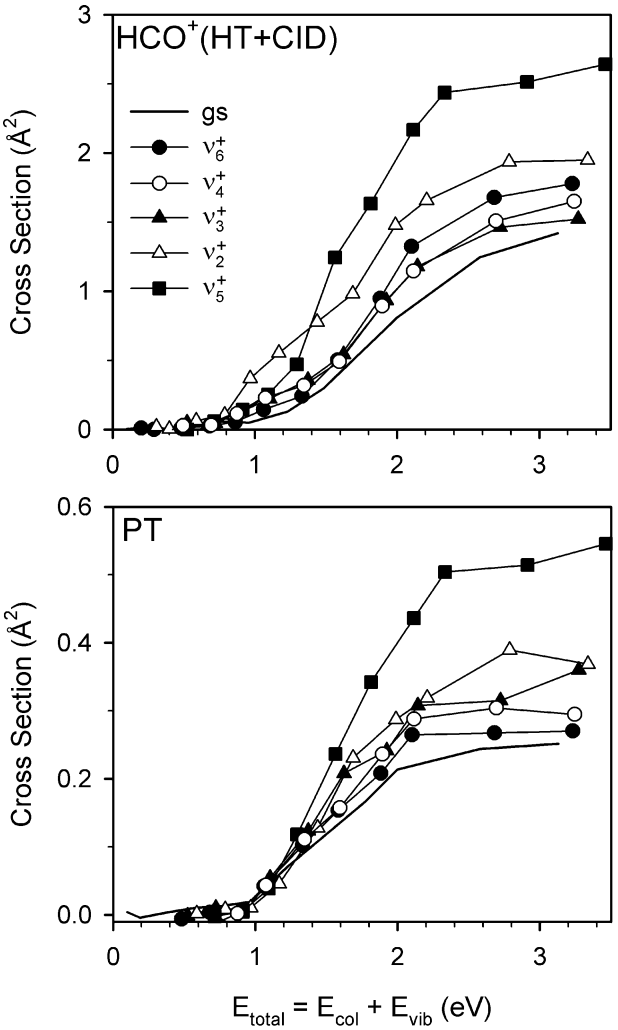

Fig. 1 Cross sections for production of HCO^+ (sum of HT and CID channels) and $OCOH^+$ (PT channel), as a function of collision energy (E_{col}) and H_2CO^+ vibrational state.

rotational energy does not vary between initial states and is small (~35 meV) compared to the width of the E_{col} distribution (~100 meV). Product ions are observed at m/z 19 and 45, corresponding to HCO^+ and $OCOH^+$. Reactions leading to these two product ions are:

$$H_2CO^+ + CO_2 \rightarrow HCO^+ + OCOH \textbf{ "HT"} \Delta_rH^\circ \geq 0.77 \text{ eV}$$

$$\rightarrow HCO^+ + H^+ + CO_2 \textbf{ "CID"} \Delta_rH^\circ = 1.09 \text{ eV}$$

$$\rightarrow OCOH^+ + HCO \textbf{ "PT"} \Delta_rH^\circ = 0.88 \text{ eV},$$

where the energetics (0 K) are taken from thermochemical data tabulated by Lias and co-workers,[20,21] except for the heat of formation for OCOH, which is a lower limit derived from an ionization energy measurement by Ruscic *et al.*[22,23] The HCO^+ product represents the sum of the HT and Collision-Induced Dissociation (CID) signals; however, as shown below, the data suggest that HT is the dominant HCO^+ production channel over the entire experimental E_{col} range. Certainly, CID does not interfere with measuring the HT appearance energy. The appearance energies for both product ions in reactions of ground state H_2CO^+ are consistent with this thermochemistry, taking into account experimental broadening factors, as discussed below. As might be expected from the fact that both channels have similar energetics and are simple atom-transfer reactions, the HCO^+ and $OCOH^+$ channels show similar E_{col} dependence. In addition, the vibrational dependence is qualitatively similar. On the other hand, the HCO^+ : $OCOH^+$ branching ratio for reaction of ground state H_2CO^+ varies between 3 : 1 and 5 : 1 as E_{col} increases from threshold to 3 eV. At collision energies just above threshold, adding vibrational excitation also shifts the branching from 3 : 1 to 5 : 1, however, because E_{vib} ranges only up to 0.337 eV (ν_5^+), the effect is larger on a per energy basis.

B. Computational results

The computational results are summarized in Fig. 2 and Table 1, where energetics are compared with the available experimental results. Generally, the G3 results are in best agreement with experimental results, and B3LYP/6-311++G** energies for known product channels are consistently 0.1–0.3 eV higher than experiment. In Fig. 2, the energetics for products are experimental, where available, and otherwise G3; and those for complexes and TS are from B3LYP/6-311++G** calculations, where all computational values are referenced to the reactant energy at the same level of theory. Three weakly bound complexes were found (A, B and C in Fig. 2). Complexes A and B both have H_2CO^+ hydrogen bonded to the O atom in CO_2, with H···O distance of 1.68 Å, and presumably can interconvert rapidly. The binding energies are 0.48 and 0.47 eV with respect to reactants, respectively. Because no rearrangement is required to form these reactant-like complexes, it is unlikely that there would be a significant activation barrier inhibiting their formation, and both might act as intermediates for the HT and PT channels. Attempts to optimize product-like complexes possessing an $[OCOH–HCO]^+$ structure instead converged to complexes A or B, indicating an absence of barriers separating complexes A and B from the HT and PT products.

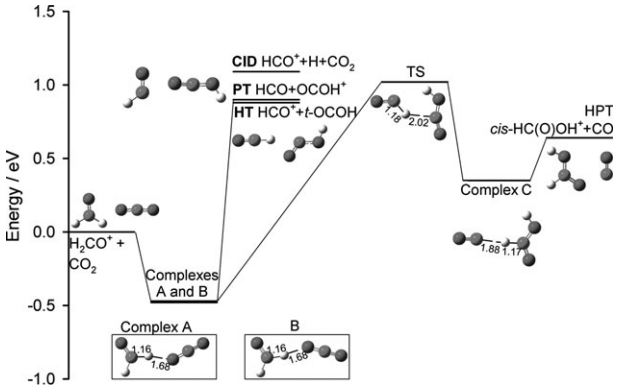

Fig. 2 Schematic reaction coordinate for $H_2CO^+ + CO_2$. Energies are derived from a combination of experimental, B3LYP/6-311++G** and G3 values, including zero point energies. The bond distances are shown in Ångstroms.

The cationic and neutral CO_2H product of the PT and HT channels could have either OCOH or branched OC(H)O structures, however, previous work[21–23] and our *ab initio* calculations indicate that the OCOH isomer is more stable and consistent with the appearance energies measured for both neutral and ionic species. Note that for the PT product ion, $OCOH^+$, the structure has the CO_2 moiety near-linear, with an H–O–C angle of 121°. For OCOH neutral, the CO_2 moiety has a more pronounced bend and there are *cis*- and *trans*-isomers, with the more stable (by 0.08 eV) *trans* form shown in Fig. 2.

The most energetically favorable product channel is formation of $CH_2O_2^+ + CO$, corresponding to HPT, *i.e.*, transfer of both H atoms and the charge from H_2CO^+ to CO_2. The analogous reaction is a major low E_{col} channel in the reaction

Table 1 Experimental and calculated Δ_rH^E (eV) relative to reactants ($H_2CO^+ + CO_2$)

	Δ_rH^E (298 K)		
Reaction energetics	B3LYP/6-311++G** [a]	G3	Experimental[b]
→ HCO^+ + *cis*-OCOH	1.34	1.10	—
→ HCO^+ + *trans*-OCOH	1.26	1.02	>0.77
→ HCO^+ + OCOH	1.74	1.66	—
→ $OCOH^+$ + HCO	1.08	0.95	0.90
→ $OCOH^+$ + HCO	5.68	5.21	—
→ *cis*-$HC(O)OH^+$ + H	0.79	—	—
→ *trans*-$HC(O)OH^+$ + H	0.77	—	0.59
→ *tc*-$C(OH)_2^+$ + H	0.56	—	0.77
→ *cc*-$C(OH)_2^+$ + H	0.92	—	—
→ *tt*-$C(OH)_2^+$ + H	0.40	—	—
→ cyclo-OCH_2O^+ + H	4.36	—	—
→ $[OH_2\cdot\cdot CO]^+$ + H	1.11	—	—
→ $CO_2^+ + H_2CO$	2.96	2.79	2.90
Complex A	−0.48	—	—
Complex B	−0.47	—	—
Complex C	0.35	—	—
TS	1.02	—	—

[a] Zero point energy calculated at B3LYP/6-311++G** was scaled by 0.9804. [b] Experimental values of Δ_rH^E (298 K) are taken from ref. 20–23

of H_2CO^+ with OCS, however, it is not seen for CO_2. The TS for this channel looks very similar to PT products, but is higher in energy and tighter than the orbiting TS that governs separation to PT products. In such a situation, it is not surprising that HPT does not compete significantly with PT. Note (Table 1) that there are six covalently bound isomers of the HPT product ion, $CH_2O_2^+$, and also one weakly bound complex with this stoichiometry. The three most important are:[22,24–27] $HC(O)OH^+$ (formic acid), $C(OH)_2^+$ (dihydroxymethylene) and OCH_2O^+. The $HC(O)OH^+$ and $C(OH)_2^+$ forms each have *cis*- and *trans*-isomers. At the B3LYP/6-311++G** level, the *tt*-$C(OH)_2^+$ isomer is most stable, however, Fig. 2 shows formic acid because it is most simply connected to the rate-limiting TS.

C. Recoil velocity distributions

The lab frame v_{axial} distributions for the $OCOH^+$ (PT) and HCO^+ (HT and CID) product ions are given in Fig. 3 and 4, respectively. Also shown as solid vertical lines in each figure are the velocities of the CM frame with respect to the lab frame, $\langle V_{CM} \rangle$, averaged over the distributions of reactant velocities. For comparison, the product velocities expected from the spectator-stripping mechanism[28] are indicated with dashed vertical lines (V_{SS}).

Axial velocity (v_{axial}) distributions are simply the projection of the full velocity distributions on the ion guide axis. Because our experiment is axially symmetric, the lab frame v_{axial} distributions can be approximately converted to the CM frame simply by subtracting $\langle V_{CM} \rangle$, allowing qualitative dynamical insights to be inferred directly from the raw lab-frame v_{axial} distributions. For example, if the reaction is mediated by a complex with lifetime ($\tau_{collision}$) greater than its rotational period ($\tau_{rotation}$), the resulting v_{axial} distribution must be symmetric about $\langle V_{CM} \rangle$. Conversely, an asymmetric v_{axial} distribution is a clear sign that reaction is direct (*i.e.*, not complex-mediated), and also reveals the dominant scattering mechanism (*i.e.*, forward *vs.* backward scattering). Finally, some insight into the partitioning of available energy into product recoil can be inferred from the displacement of the v_{axial} distributions from $\langle V_{CM} \rangle$. There are a few limitations of this technique, as implemented here. Product ions that are strongly backscattered in the CM frame may have negative laboratory velocities. To collect such ions, the ion lens at the ion guide entrance is biased positive relative to the guide potential, reflecting these ions back toward the detector. The reflected ions appear at long flight times, corresponding to low but positive lab velocities. In addition, the slowest ions are most likely to have their velocities distorted by small inhomogeneities in the surface potentials on the ion guides. Finally, these distortions in the low velocity portion of the v_{axial} distributions are exacerbated by the singular TOF-to-velocity Jacobian. For this system, only the PT channel gives ions backscattered to low lab velocity, and even there, we are still able to measure all but the low v_{axial} tail of the distribution. In fitting the distributions, data points at velocities below 450 m s^{-1}, where the measurements are problematic, are given zero weight.

At high E_{col}, the distributions for PT (Fig. 3) are strongly asymmetric with respect to $\langle V_{CM} \rangle$, indicating a direct reaction

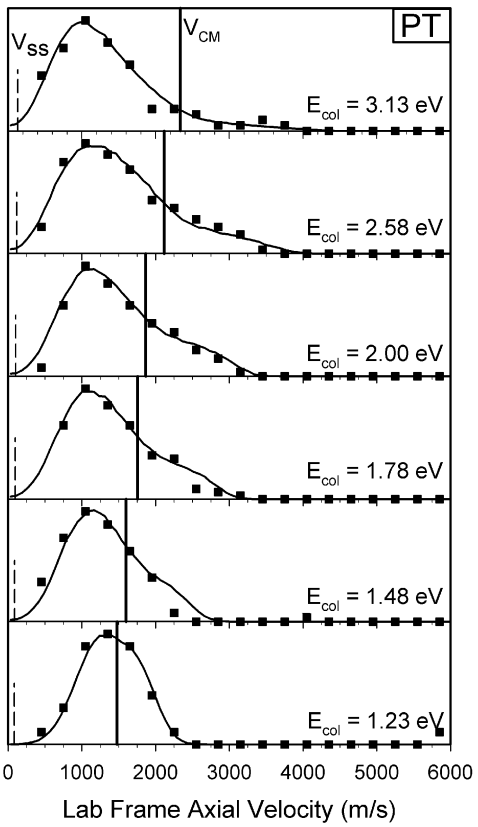

Fig. 3 Axial recoil velocity distributions for the PT product ions ($OCOH^+$). ■: experimental data; —: simulations based on the osculating complex model; |: lab velocity of the CM frame ($\langle V_{CM} \rangle$); ¦: spectator-stripping limit velocity (V_{SS}).

mechanism with $\tau_{collision} \ll \tau_{rotation}$. Because we define "forward" and "backward" scattering as product *ions* with axial velocities faster or slower, respectively, than $\langle V_{CM} \rangle$, the backward-peaked v_{axial} distributions for PT correspond to proton transfer occurring without substantial deflection of the collision partners. The most likely mechanism for such scattering is proton stripping occurring in large impact parameter (b) collisions, consistent with the observation that v_{axial} approaches the spectator-stripping limit at high energies. There is also a tail extending into the forward direction, suggesting that small impact parameter collisions also contribute to PT, albeit with low probability, leading to rebounding product ions. Note that the cross section for PT never exceeds ~1% of the hard sphere cross section (~30 $Å^2$), *i.e.*, although PT occurs in large b collisions, the efficiency is quite low, even for E_{col} well in excess of the endoergicity.

As E_{col} is reduced , the peak of the v_{axial} distributions for PT shifts toward $\langle V_{CM} \rangle$, approaching forward–backward symmetry at the lowest E_{col} measured. Note, however, that for E_{col} near the threshold energy for an endoergic reaction, the recoil velocities are necessarily low, and it becomes increasingly difficult to resolve asymmetries, given the broadening resulting from the experimental distributions of reactant velocities.

Because the charge is not transferred in producing HCO^+ (HT + CID, Fig. 4), the forward-peaked v_{axial} distributions

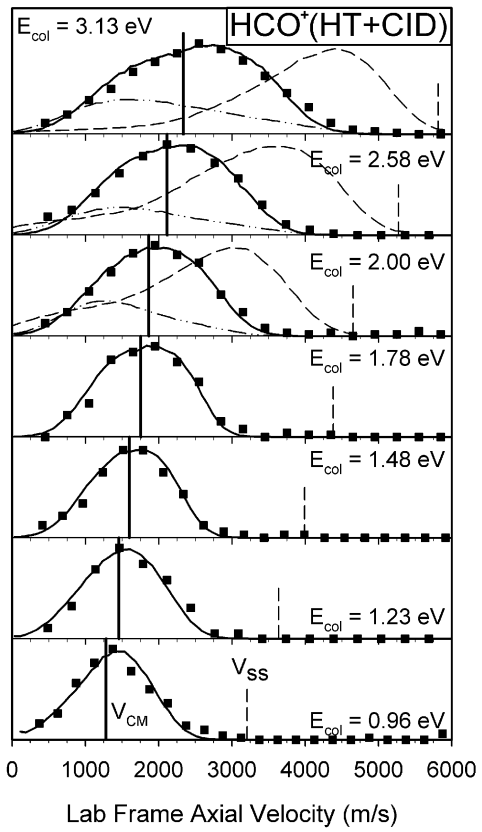

Fig. 4 Axial recoil velocity distributions for the HCO^+ product at selected collision energies. ■: experimental data; —: simulations based on the osculating complex model; ¦: lab velocity of the CM frame ($\langle V_{CM}\rangle$); ¦: spectator-stripping limit velocity (V_{SS}); --: distribution that would result if the recoil dynamics were the same as in the PT channel; ---: v_{axial} distribution for HCO^+ production in CID of H_2CO^+ with Ne.

correspond to low deflection angle scattering, as was also seen for PT. Note, however, that the product recoil dynamics are very different from the stripping behavior observed for PT at high E_{col}. To emphasize this point, the top few frames of Fig. 4 show what the HCO^+ distributions would look like if the scattering dynamics were identical to that in the PT channel. These "PT-like" distributions are obtained by reflecting the PT distributions through $\langle V_{CM}\rangle$ (to account for the fact that the charge is not transferred in HCO^+ production) then scaling the velocities to account for the difference product mass ratios between HCO^+ and PT. Clearly, the experimental HCO^+ distributions are much less asymmetric than the analogous PT distributions and peak closer to $\langle V_{CM}\rangle$, corresponding to much lower recoil energy.

One complication in analyzing the HCO^+ data is that there may be a significant contribution from CID, as well as the HT reaction of interest. While it is not possible to separate these two contributions quantitatively (except for $E_{col} < 1.09$ eV—the threshold for CID), we can make use of our earlier study of H_2CO^+ dissociation in collisions with Ne and Xe to estimate the CID contribution.[4] For Ne, the CID cross section rises slowly from threshold, reaching only $\sim$0.5 Å^2 by E_{col} = 3 eV. For Xe, the cross section has sharper E_{col} dependence, and reaches $\sim$1.8 Å^2 at E_{col} = 3 eV. The CID cross section well above threshold is determined by the efficiency of collision-to-internal energy ($T \rightarrow E_{internal}$) conversion, and it is unclear how CO_2 might compare with Xe and Ne as a collision partner. Its mass lies closer to Ne than to Xe, but its polarizability (2.9 Å^3) is closer to that for Xe (4.0 Å^3) than Ne (0.4 Å^3). Another factor likely to influence $T \rightarrow E_{internal}$ conversion is the fact that CO_2 has rotational and vibrational degrees of freedom that will tend to be collisionally excited, competing with H_2CO^+ in the partitioning of final internal energy.

Fortunately, the v_{axial} distributions provide a way to estimate, at least qualitatively, the contribution of CID to the HCO^+ signal. When scattering kinematics (*i.e.*, mass ratios) are accounted for, the CID product v_{axial} distributions for both Ne and Xe are similar—broadly backward-peaked at all E_{col}, with a significant tail extending into the forward direction. A combination of modelling[4] and trajectory analysis[29] revealed that CID occurs over a broad range of impact parameters, but most efficiently at small impact parameters, leading to rebounding products. For reference, the top few frames of Fig. 4 give the v_{axial} distributions for HCO^+ generated by Ne CID, shifted and velocity-scaled appropriately to compensate for the higher mass of CO_2. In each case, the Ne CID data have been intensity-scaled so that the low lab velocity (*i.e.*, high recoil velocity) tail approximately matches that of the HCO^+ (HT + CID) data for reaction with CO_2. To the extent that CID recoil dynamics is similar for Ne and CO_2, comparison of the two data sets suggests that CID might account for about half the back-scattered HCO^+ and for 30–40% of the total HCO^+ production at the three compared collision energies. At lower E_{col}, the v_{axial} distributions are too featureless to allow this approach to estimating the CID contribution, however, it is reasonable to assume that the contribution from CID decreases to zero as E_{col} approaches the CID threshold (1.09 eV). If this presumed back-scattered HCO^+ from CID is subtracted from the v_{axial} distributions, the corrected distributions are clearly more forward-peaked. Note, however, that even with this correction, the HT distributions at high E_{col} are not nearly as asymmetric (forward : backward ratio $\sim$2.5) as those for PT (backward : forward ratio $\sim$10). Furthermore, the HT distributions still peak closer to V_{CM} than V_{SS}. The implication is that there is considerably more conversion of E_{col} to product internal energy, with correspondingly lower recoil energy, for HT compared to PT.

To correct the v_{axial} distributions for experimental broadening resulting from the velocity distributions of both reactants, the data were fit using a simulation of the experiment described previously.[10] The simulation requires input from a model describing the recoil dynamics, and for this purpose we used a three parameter model based on the osculating complex model.[30] In this model, a short-lived collision complex is assumed to form, with rotational period ($\tau_{rotation}$). The collision complex is assumed to decay to products with a lifetime, $\tau_{collison}$, and recoil energy distribution, P(E_{recoil}). The degree of forward–backward symmetry in the distributions depends only on the ratio $\tau_{collision}/\tau_{rotation}$. The collision time can be put on an absolute scale by estimating $\tau_{rotation}$ from the moment of inertia and angular momentum of the complex, the latter estimated from the magnitude of the cross section

Table 2 Product ion velocity distribution fit results for $H_2CO^+ + CO_2$

E_{col} eV^{-1}	$\langle E_{avail}\rangle$[a] eV^{-1}	$\langle E_{recoil}\rangle$ eV^{-1}	$\langle E_{recoil}\rangle/\langle E_{avail}\rangle$ (%)	$\tau_{collision}$/ ps	$\tau_{fly\text{-}by}$[b]/ ps
HCO^+ (HT + CID)					
0.96	0.19	0.11	58	1.10	0.155
1.23	0.39	0.12	31	1.04	0.137
1.48	0.63	0.12	19	1.0	0.125
1.78	0.93	0.14	15	1.0	0.114
2.00	1.16	0.21	18	0.89	0.108
2.58	1.73	0.25	14	0.83	0.095
3.13	2.28	0.36	16	0.55	0.086
$OCOH^+$ (PT)					
1.23	0.40	0.15	38	0.82	0.137
1.48	0.62	0.35	56	0.31	0.125
1.78	0.90	0.51	57	0.26	0.114
2.00	1.15	0.63	55	0.26	0.108
2.58	1.74	0.93	53	0.18	0.095
3.13	2.27	1.30	57	0.10	0.086

[a] $\langle\ \rangle$ = mean value. [b] $\tau_{fly\text{-}by}$ defined as time for undeflected reactants to travel a relative distance of 5.0 Å.

and E_{col}. Assuming a complex like A in Fig. 2, forming with the capture cross section,[31] $\tau_{rotation}$ drops smoothly from ~1.2 ps at E_{col} = 1.0 eV to 0.9 ps at E_{col} = 3.2 eV. Here, P(E_{recoil}) is assumed to be a Gaussian distribution parameterized by a peak value and width defined in terms of the available energy (E_{avail}) for the product channel of interest. The solid curves shown in Fig. 3 and 4 are the fits, and the numerical results are summarized in Table 2.

As shown in Table 2, $\tau_{collision}$ for PT drops rapidly with increasing E_{col}, reflecting the increasingly asymmetric v_{axial} distributions. As an indication of the collision time that might be expected in the limit of a direct mechanism, Table 2 also gives $\tau_{fly\text{-}by}$, taken as the time required for reactants to move a relative distance of 5 Å. For PT, $\tau_{collision}$ exceeds $\tau_{fly\text{-}by}$ at low E_{col}, but becomes comparable by E_{col} ~ 2.5 eV. Clearly, any complexes that dominate PT are short-lived, except possibly at E_{col} near threshold. It should be noted that in the osculating complex model, the degree of forward–backward symmetry is assumed to result entirely from rotation of a collision complex. In the high E_{col} limit, where $\tau_{collision}$ is negligible, the shape of the v_{axial} distributions is more sensitive to the distribution of impact parameters contributing to each product channel, with small impact parameters leading to rebounding, and large impact parameters leading to stripping, as discussed above.

For HCO^+ (sum of HT and CID), $\tau_{collision}$ drops more slowly with increasing E_{col}, reflecting the more symmetric distributions. The distributions are almost certainly more asymmetric once the contribution from CID is subtracted, thus, the true $\tau_{collision}$ values should be shorter than those given in Table 2. As discussed above, however, it is unlikely that the corrected HT distributions are nearly as asymmetric as those for PT, even at our highest E_{col}. Because we only know the qualitative shape of the CID contribution, we have not attempted to analyze this correction quantitatively.

Table 2 also includes estimates of the average energy partitioned into recoil, $\langle E_{recoil}\rangle$, extracted from the fits. For PT, the $\langle E_{recoil}\rangle$ values extracted should be lower limits on the true values, because ions with low lab velocities (*i.e.*, high CM velocities) are excluded from the fits. The tables give both $\langle E_{recoil}\rangle$ and the fraction of available energy (E_{avail}) going into recoil ($\langle E_{recoil}\rangle/\langle E_{avail}\rangle$). For PT, $\langle E_{recoil}\rangle$ increases with increasing E_{col}, such that $\langle E_{recoil}\rangle/\langle E_{avail}\rangle$ is roughly constant at ~55%, except near threshold. For HCO^+ (*i.e.*, HT + CID), $\langle E_{recoil}\rangle$ is small and increases slowly with E_{col}, such that the fraction of E_{avail} partitioned to recoil is below 20%, except at energies near threshold. It should be noted that the effect of the presumed CID contribution on the $\langle E_{recoil}\rangle$ values should be small, because the correction is expected to mainly affect the symmetry of the distributions, not the displacement of the peaks from $\langle V_{CM}\rangle$. The implication is that in the HT channel, most of the available energy is in product $E_{internal}$, whereas for PT, ~55% is partitioned to recoil.

Velocity distributions were also measured for the reaction of vibrationally excited H_2CO^+. These are not shown, as they are qualitatively quite similar to those for ground state reactants. The similarity reflects the fact that E_{recoil} depends mostly on E_{avail} and on the collisional energy transfer dynamics. For the energies relevant to this system, E_{avail} mostly depends on E_{col}, and apparently vibrational excitation does not strongly affect energy transfer. For the PT channel, the v_{axial} distributions broaden slightly, and their peak shifts slightly to lower lab velocity (higher CM frame velocity). Based on the discussion above, and on the observed vibrational enhancement of the PT cross section (Fig. 1), the implication is that vibrational excitation increases the probability of PT in large impact parameter collisions, although the efficiency remains quite small. For the HCO^+ channel, the effect on the v_{axial} distributions at high E_{col} is insignificant, and there is only a small broadening of the distributions at low E_{col}, presumably reflecting the increase in available energy from the vibrational excitation.

D. Vibrational effects

While vibration has little effect on product recoil, there are substantial cross section enhancements and changes in product branching. Fig. 1 compares the effects of vibrational state and collision energy. Fig. 5 shows the vibrational enhancement factors *vs.* E_{vib} for two ranges of E_{col}. Each E_{vib} value corresponds to one of the six states studied, as indicated by the data point labels. The enhancement factor is calculated as the ratio of the cross section for the reaction of a particular state, $\sigma(\nu^+)$, to the ground state cross section, σ(gs). To reduce statistical uncertainty in the ratios of the rather small cross sections for this system, data for the indicated ranges of E_{col} have been averaged. The error bars shown reflect the reproducibility of the ratios, and are larger for the smaller PT cross section, as expected. As shown, both PT and HCO^+ production are strongly enhanced by vibrational excitation, and the enhancements are roughly proportional to E_{vib}. The lack of strong vibrational mode dependence is unusual. Most reactions of $H_2CO^+(\nu^+)$ show significant mode effects on reactivity and/or product branching (see, for example, reactions with C_2H_2,[32] C_2D_4,[33] OCS,[34] and ND_3.[35]).

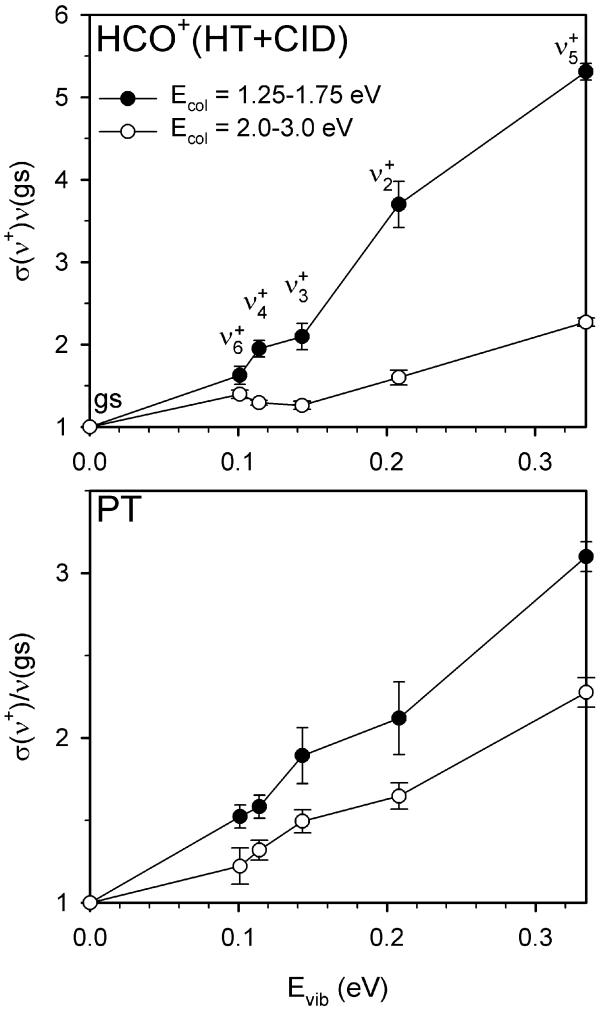

Fig. 5 Vibrational enhancement factors *vs.* E_{vib}, for different E_{col} ranges, for the HT and PT reactions.

IV. Discussion

A. Reaction mechanism

1. Complex-mediated *vs.* direct reaction. One question is whether complexes A and B (Fig. 2) might be stable enough to significantly mediate the HT and PT reactions, at least for energies near threshold, where the energy available to products is low and the velocity distributions are roughly forward–backward symmetric. We calculated the decay rate of complexes A and B to PT and HT products, and also back to reactants. As might be expected from the endoergicities of both PT and HT channels, decay of both complexes is dominated by dissociation back to reactants, *i.e.*, no reaction. For E_{avail} just above the PT and HT thresholds, and for large values of the angular momentum (L)—corresponding to complexes formed near the capture collision limit—the centrifugal barrier for dissociation back to reactants is high enough to result in complex lifetimes on the order of a few picoseconds, comparable to $\tau_{collision}$, Table 2. Such collisions are irrelevant, however, because large L leads to centrifugal barriers in the PT and HT channels as well, rendering such collisions non-reactive. In other words, within the energy available in the endoergic channels, it is not possible for products to recoil fast enough to conserve L for collisions near the capture limit. Conversely, for smaller L collisions, where the PT and HT channels are accessible, the complex lifetimes are only ~30 fs, even at threshold, because decay back to reactants is so fast. This time scale is considerably shorter than $\tau_{fly\text{-}by}$, thus the lifetime of any statistical complexes is insignificant for all energies above the reaction thresholds.

Even if we were to ignore the issue of complex lifetime, the RRKM results indicate that the branching to HT and PT products for all L and all E_{col} is less than 1%, compared to the experimental reaction efficiency, which reaches ~6%. Finally, if even the dominance of decay back to reactants is ignored, the HT : PT branching is calculated to favor the PT channel over most of the E_{col} range (see next section), whereas HT clearly dominates experimentally. Based on all these considerations, we can conclude that the products we observe result entirely from a direct mechanism, *i.e.*, that any collision complexes that might form are too short-lived to behave statistically. The apparently forward–backward v_{axial} distributions at low E_{col} simply reflect the fact that the recoil energy is necessarily small near threshold, making it difficult to resolve any asymmetries.

2. Branching ratio and collision energy dependence

Over the E_{col} range studied, the HCO^+/PT branching ratio ranges from ~3 : 1 to ~4 : 1, if we make the approximate correction for CID discussed above. The predominance of HT products is surprising in that the difference in HT and PT channel energies is small compared to E_{col}, particularly for the upper end of our E_{col} range. In addition, the geometry of the PT products is more reactant-like than that of the HT products, and we might expect that this factor should also favor PT. Formally, the HT (HCO^+ + OCOH) and PT (HCO + $OCOH^+$) channels are just the two lowest electronic states, *i.e.*, charge states, of $(HCO + OCOH)^+$. Note, however, that the geometries of both HCO and OCOH are quite different in the HT and PT charge states. As shown in Fig. 2, HCO is bent, HCO^+ is linear, and the OCO bend angle in OCOH is also very different in the neutral and cationic species. As a consequence, at the equilibrium geometry of the PT products (HCO + $OCOH^+$), the HT products (HCO^+ + OCOH) are 3.76 eV higher in energy at the B3LYP/6-311++G** level. Similarly, at the HT product geometry, the PT products lie 3.2 eV higher in energy. In essence, the HT and PT product channels represent two distinct exit valleys on the lowest Born–Oppenheimer potential energy surface, displaced along a coordinate corresponding to the geometry change between HT and PT product structures. The two exit valleys are presumably separated by a significant barrier resulting from the avoided crossing of the two diabatic surfaces.

The RRKM calculations discussed above clearly rule out a complex-mediated mechanism, however, it is not inconceivable that statistical factors might still control branching between the HT and PT charge states. In such a mechanism, HT : PT branching should be determined by the ratio of accessible

ro-vibrational levels belonging to the HT and PT valleys on the surface.[36] Based on structures and scaled vibrational frequencies from our B3LYP/6-311++G** calculations, we note that the vibrational frequency distribution and rotational constants for OCOH and $OCOH^+$ are similar. In comparing HCO^+ to HCO, however, the degenerate bend mode (825 cm^{-1}) in linear HCO^+ becomes a higher energy bend (1058 cm^{-1}) and a much lower energy rotation (B = 24 cm^{-1}) in neutral HCO. The net effect is that the sum of states in the HT channel is lower than in the PT channel, except very near threshold, where the lower HT endoergicity becomes the dominant factor. The HT : PT branching is predicted to vary from ~1 : 1.1 for E_{col} near 1 eV, to 1 : 1.7 at E_{col} = 3 eV—in poor agreement with the observed ratio variation from 4 : 1 to 5 : 1 (or 3 : 1 to 4 : 1 with the estimated CID correction).

It appears, therefore, that the HT : PT branching must be under dynamical control, *i.e.*, trajectories taken by reactive collisions tend to carry the system into the HT exit valley about ~3–4 times more often than into the PT valley. Recall that the v_{axial} distributions show that the HT products have much higher internal energies than PT products, and that the dynamics of PT approach stripping behavior. Taking the absolute magnitudes of the cross section into account, we can describe the mechanism as follows. Trajectories at large impact parameter are nearly all non-reactive, but the small fraction that react (<1% for ground state reactants) predominantly form PT products *via* a proton stripping process, wherein the geometry undergoes minimal distortion and the available energy is partitioned largely to product recoil. Trajectories at small impact parameters react with somewhat higher efficiency (<5%), and convert most of the available energy to product vibration and rotation. These harder, more intimate collisions largely generate HT products. The decrease in v_{axial} distribution asymmetry for both PT and HT as E_{col} decreases indicates that, for E_{col} near threshold, both channels require more intimate collisions to drive the necessary energy conversion to overcome the endoergicity.

Given that PT and HT appear to result from different types of collisions, at least in the above-threshold energy range, it is interesting that the E_{col} and vibrational state dependence of the two channels is so similar. The vibrational effects are discussed below; here we will concentrate on collision energy effects. A model commonly used to think about the E_{col} dependence of endoergic reactions is the line-of-centers model.[37] Here, it is assumed that only the line-of-centers energy ($E_{loc} = {}^1/_2 \cdot \mu \cdot v_{loc}^2$) is effective in overcoming the endoergicity, because the rest of the collision energy must remain in translation in order to conserve angular momentum. In the expression for E_{loc}, μ is the usual reduced mass and v_{loc} is the projection of the reactants' relative velocity on the line separating the centers of mass of the two reactants, at their point of closest approach (usually approximated as a hard sphere of separation d). For collisions at an impact parameter b, the line-of-centers energy is: $E_{loc} = E_{col} \cdot (1 - (b/d)^2)$. For a reaction with a threshold energy, E_0, the range of b where E_{loc} exceeds E_0 increases with E_{col}, therefore the cross section has the following E_{col} dependence for $E_{col} > E_0$: $\sigma_{loc} = \sigma_{HardSphere} \cdot (E_{col} - E_0)/E_{col}$. This form of the cross section rises linearly from E_0, then asymptotically approaches the hard sphere cross section as E_{col} becomes large compared to E_0. Based on this model, we would expect the HT and PT cross sections to have similar energy dependence, because they have nearly identical values of E_0 (0.88 and 0.9 eV, respectively (next section)). The most obvious discrepancy is that for E_0 = 0.9 eV, σ_{loc} reaches ~72% of $\sigma_{HardSphere}$ at 3.2 eV, whereas the experimental ground state total cross section (sum of PT and HCO^+) is only ~6% of $\sigma_{HardSphere}$ (~30 $Å^2$) by this energy. The low experimental cross section might be rationalized as evidence for some bottleneck that inhibits reaction—a steric requirement, for example.

The other factor to consider is that the v_{axial} distributions suggest that PT occurs in collisions with larger impact parameters than HT, at least for high E_{col}. Because the relation between E_{col} and E_{loc} depends on b, this b-dependent branching should result in different E_{col} dependence for the HT and PT channels. In particular, for a channel that occurs mostly at large impact parameters, the probability for collisions with $E_{loc} > E_0$ only becomes large for E_{col} well above E_0. The line-of-centers PT cross section should, therefore, rise slowly from threshold, only becoming significant for E_{col} well above E_0. HT, which appears to occur in small b collisions at all E_{col}, should have a cross section that rises rapidly from threshold, but levels off sooner than σ_{PT}. Comparison of the ground state cross sections for PT and HCO^+ in Fig. 1, as well as the fitting analysis in Table 2, shows that this is clearly not the case. If anything, σ_{PT} approaches its high E_{col} asymptote faster than σ_{HCO+}.

B. Vibrational effects

Fig. 1 shows the E_{col} and H_2CO^+ vibrational state dependence of σ_{HCO+} and σ_{PT}. An obvious question is how vibration compares to E_{col} in driving the endoergic reactions. Vibrational effects at high energies are determined by the *average* effect of vibration on reactivity, while those on the threshold energies are a measure of whether there are *any* collisions that are able to utilize the vibrational energy in overcoming the endoergicity. We first discuss the behavior near threshold.

1. Behavior near threshold. The data in Fig. 1 are plotted as a function of $E_{total} = E_{col} + E_{vib}$, thus if E_{vib} and E_{col} contribute with equal efficiency to overcoming the reaction endoergicity, the curves in each frame of the figure should all converge on a common appearance energy. Within the limitations of such analysis and the experimental uncertainties inherent in studying inefficient reactions near threshold, this appears to be the case. To make the comparison more quantitatively, we fit the experimental E_{col} dependence of the cross sections for each vibrational state, convoluting a model "true" $\sigma(E_{col})$ function with the appropriate experimental broadening distributions that result from ion beam energy spread and thermal motion of the CO_2 target. For the "true" $\sigma(E_{col})$ function, we have taken the usual modified line-of-center model:[2,3]

$$\sigma(E_{col}) = \sigma_0 \frac{(E_{col} + E_{vib} + E_{rot} - E_0)^n}{E_{col}}$$

for $(E_{col} + E_{vib} + E_{rot}) > E_0$, otherwise $\sigma(E_{col}) = 0$. Here E_0 is the threshold energy, and n is a parameter controlling

curvature of the cross section function. E_{vib} and E_{rot} are the vibrational and rotational energy of the reactants, and σ_0 is a normalization factor adjusted to match the magnitude of the experimental cross section at some E_{col} well above threshold. The model $\sigma(E_{col})$ function is run through a Monte Carlo simulation of the experiment to factor in the broadening functions, and the n and E_0 parameters are adjusted until the convoluted model function matches the experiment. For the CO_2 target, the translational and rotational energies are sampled from thermal distributions at room temperature. For H_2CO^+, we measure the translational energy spread by TOF, E_{vib} is well determined, and E_{rot} is negligible because our ions are produced by REMPI of a supersonic beam. The best-fit values of E_0 for reaction of ground vibrational state H_2CO^+ are 0.88 and 0.90 eV for HT and PT, respectively, with estimated fitting precision of $\pm$0.03 eV. By including uncertainties relating to the shape of the primary beam translational energy distribution, we estimate that the accuracy of the E_0 values is $\sim\pm$0.06 eV. The PT value (0.90 eV) is consistent with the value (0.88 eV) derived in the thermochemical literature discussed above, and for HT the value (0.88 eV) is also consistent in the sense that it is above the lower limit estimated for that channel from literature values ($>$0.77 eV).

To focus on the issue of the relative effectiveness of E_{vib} and E_{col}, it is useful to minimize the number of adjustable parameters in the fits; thus, in fitting the data for vibrationally excited H_2CO^+, E_0 was fixed at values extracted in the ground state fits. E_{vib} is nominally the energy of the selected H_2CO^+ state, however, for the purpose of comparing the effects of E_{col} to vibrational energy in different modes, we treated E_{vib} as a fitting parameter. As σ_0 is simply a scale factor, not affecting the threshold or curvature, the only parameters affecting the fit are n and E_{vib}. Table 3 gives the results. The major result is that the fitted E_{vib} values are essentially equal to the actual vibrational state energies, which means that near the HT and PT thresholds, all modes of vibrational excitation have equal effectiveness at driving reaction, and vibrational and collision energy are also equivalent in this respect. While equivalence of all forms of energy is anticipated in the form of the "true" $\sigma(E_{col})$ function above, it is far from universal. In some systems, vibration is less effective at threshold than E_{col},[38] and in others, where E_{col} does not drive reaction at threshold, E_{vib} may be more effective.[6]

2. Behavior at above-threshold energies. As shown in Fig. 5, the effects of vibration are approximately proportional to E_{vib}, in both E_{col} ranges examined. For E_{col} between 1.25 and 1.75 eV, where we observe the maximum slope of cross section *vs.* E_{col}, we can compare the relative effectiveness of vibrational and collision energy by comparing the slope of the cross section enhancements. For ground state reactants, when E_{col} increases from 1.25 to 1.75 eV, the HCO^+ cross section increases by a factor of $\sim$4.5, corresponding to a slope of a factor of $\sim$9 eV^{-1}. The E_{col} enhancement slope for PT is similar. In contrast, the vibrational enhancement slope is a factor of $\sim$15.5 eV^{-1} for HCO^+ and a factor of $\sim$9.3 eV^{-1} for PT, averaged over E_{col} between 1.25 and 1.75 eV. In other words, vibrational and collision energy are about equally efficient in driving the PT reaction in this energy range as they were in the threshold energy range. For HCO^+, in contrast, vibration is about 60% more effective than collision energy.

For $E_{col} \geq$ 2 eV, where both HCO^+ and PT cross sections have weak dependence on E_{col} (Fig. 1), both channels are vibrationally enhanced with a slope corresponding to a factor of $\sim$6.5 eV^{-1} of E_{vib}. In essence, the E_{col} enhancement of these endoergic reactions saturates for $E_{col} >$ $\sim$2 eV, whereas vibrational excitation continues to have a substantial effect, even though the vibrational state energies are all small compared to the available energy. When E_{col} is raised, there is a concomitant increase in the angular momentum and collision velocity, the latter leading to a decrease in the collision time scale. In this system, where the reactant and product reduced masses are similar, it is unlikely that there are any unusual angular momentum effects; however, decreasing collision time and increasingly impulsive interactions may offset the expected enhancement from increasing E_{col}. In contrast, when E_{vib} is increased there is no change in collision velocity or angular momentum. Furthermore, because we excite the H_2CO^+ reactant, the vibrational energy is added directly to the molecule containing the bond to be broken.

Close examination of Fig. 5 shows some hint of mode specific effects, although the mode specificity is much smaller than we have observed in other reactions of H_2CO^+, such as those with C_2D_4,[33] C_2H_2,[32] OCS,[34] and ND_3.[35] Interestingly, the mode dependence of the PT and HCO^+ channels is complementary. Note, for example, that for HCO^+ at E_{col} in the 1.25–1.75 eV range, ν_4^+ and ν_2^+ give enhancements larger than might be expected from the overall trend, while the same modes give smaller than expected enhancements for the PT channel. In essence, while all modes strongly enhance both product channels, some modes (ν_4^+ = out-of-plane bend, ν_2^+ = CO stretch) slightly favor HCO^+, and some (ν_6^+ = in-plane CH_2 rock, ν_3^+ = CH_2 scissors, ν_5^+ = asym CH stretch) favor PT. Given that the branching between the HT and PT charge states appears to be controlled by dynamics (see above), the implication is that certain modes tend to push the system toward one exit valley or the other.

To some extent, complementary mode effects on competing channels is not surprising. For example, in the reaction of H_2CO^+ with C_2D_4[33] and with C_2H_2,[32] we observed that PT is enhanced by all vibrational modes, and the competing HT channel is actually inhibited by vibrational excitation. In those reactions, the difference is that HT and PT are both exoergic channels with large cross sections, and the total cross section approaches the collision limit. In such systems, if vibration

Table 3 Integral cross section fit results using the modified line-of-centers model

		E_{vib} (fit)		E_{vib}(fit)/E_{vib}(actual)%		n	
Ionic state	E_{vib} (actual)	HT	PT	HT	PT	HT	PT
Ground state	0	0	0	—	—	1.95	1.45
$\nu_6^+ = 1$	101	101	101	100	100	2.00	1.30
$\nu_4^+ = 1$	114	114	111	100	97	1.35	1.30
$\nu_3^+ = 1$	143	143	143	100	100	1.40	1.30
$\nu_2^+ = 1$	208	208	208	100	100	1.10	1.50
$\nu_5^+ = 1$	337	330	320	98	95	1.70	1.60

strongly enhances one channel, the enhancement must come at the expense of the competing channels. In the present system, HT and PT are formally in competition with each other, however, the overwhelmingly dominant channel is non-reactive scattering, corresponding to >94% of all collisions over the entire energy range. Here, H_2CO^+ vibrational excitation enhances both product channels, with the intensity predominantly coming out of the non-reactive scattering channel, with only a small competitive effect on the mode dependence of the two channels.

It is interesting to note that for the reactions with C_2H_2 and C_2D_4, excitation of ν_4^+ and ν_2^+ results in larger-than-expected enhancements of the PT channel, but also cause smaller-than-expected inhibitions of the competing HT channel. In other words, ν_4^+ (out-of-plane bend) and ν_2^+ (CO stretch) excitation increases the total probability for transferring H and H^+. These are also the two modes that give the largest enhancements for the total cross section (PT + HCO^+) in this system, therefore, we can conclude that these modes tend to enhance transfer of H/H^+ from H_2CO^+ to various receptor molecules. It is not obvious how either of these modes is coupled to the H/H^+ transfer reaction coordinate, which is most obviously related to ν_5^+ (asym CH stretch). On the other hand, in a trajectory study of H_2CO^+ collisions with Ne,[29] we showed that ν_4^+ excitation resulted in higher-than-expected efficieny of collision-to-internal energy conversion (ν_2^+ was not studied), and such energy conversion is likely to be important in driving reaction.

Acknowledgements

This work was supported by the National Science Foundation under Grant No. CHE-0110318.

References

1 N. G. Adams, D. Smith and D. Grief, *Int. J. Mass Spectrom. Ion Processes*, 1978, **26**, 405.
2 P. B. Armentrout, *Int. J. Mass Spectrom.*, 2000, **200**, 219.
3 M. B. Sowa-Resat, P. A. Hintz and S. L. Anderson, *J. Phys. Chem.*, 1995, **99**, 10736.
4 J. Liu, B. Van Devener and S. L. Anderson, *J. Chem. Phys.*, 2002, **116**, 5530.
5 B. Yang, Y. H. Chiu, H. Fu and S. L. Anderson, *J. Chem. Phys.*, 1991, **95**, 3275.
6 J. Liu, B. W. Uselman, J. M. Boyle and S. L. Anderson, *J. Chem. Phys.*, 2006, **125**, in press.
7 J. Liu, K. Song, W. L. Hase and S. L. Anderson, *J. Phys. Chem. A*, 2005, **109**, 11376.
8 J. Liu, B. V. Devener and S. L. Anderson, *J. Chem. Phys.*, 2003, **119**, 200.
9 J. Liu, K. Song, W. L. Hase and S. L. Anderson, *J. Am. Chem. Soc.*, 2004, **126**, 8602.
10 Y.-H. Chiu, H. Fu, J.-T. Huang and S. L. Anderson, *J. Chem. Phys.*, 1995, **102**, 1199.
11 Y.-H. Chiu, H. Fu, J.-T. Huang and S. L. Anderson, *J. Chem. Phys.*, 1996, **105**, 3089.
12 Y.-H. Chiu, PhD thesis, State University of New York at Stony Brook, 1996.
13 R. Spence and W. Wild, *J. Chem. Soc.*, 1935, **338**.
14 F. S. Dainton, K. J. Ivin and D. A. G. Walmsley, *Trans. Faraday Soc.*, 1959, **55**, 61.
15 J. Liu, H.-T. Kim and S. L. Anderson, *J. Chem. Phys.*, 2001, **114**, 9797.
16 D. Gerlich, *Adv. Chem. Phys.*, 1992, **82**, 1.
17 M. J. Frisch, G. W. Trucks, H. B. Schlegel, G. E. Scuseria, M. A. Robb, J. R. Cheeseman, J. J. A. Montgomery, T. Vreven, K. N. Kudin, J. C. Burant, J. M. Millam, S. S. Iyengar, J. Tomasi, V. Barone, B. Mennucci, M. Cossi, G. Scalmani, N. Rega, G. A. Petersson, H. Nakatsuji, M. Hada, M. Ehara, K. Toyota, R. Fukuda, J. Hasegawa, M. Ishida, T. Nakajima, Y. Honda, O. Kitao, H. Nakai, M. Klene, X. Li, J. E. Knox, H. P. Hratchian, J. B. Cross, C. Adamo, J. Jaramillo, R. Gomperts, R. E. Stratmann, O. Yazyev, A. J. Austin, R. Cammi, C. Pomelli, J. W. Ochterski, P. Y. Ayala, K. Morokuma, G. A. Voth, P. Salvador, J. J. Dannenberg, V. G. Zakrzewski, S. Dapprich, A. D. Daniels, M. C. Strain, O. Farkas, D. K. Malick, A. D. Rabuck, K. Raghavachari, J. B. Foresman, J. V. Ortiz, Q. Cui, A. G. Baboul, S. Clifford, J. Cioslowski, B. B. Stefanov, G. Liu, A. Liashenko, P. Piskorz, I. Komaromi, R. L. Martin, D. J. Fox, T. Keith, M. A. Al-Laham, C. Y. Peng, A. Nanayakkara, M. Challacombe, P. M. W. Gill, B. Johnson, W. Chen, M. W. Wong, C. Gonzalez and J. A. Pople, Gaussian, Inc., Pittsburgh, PA, 2003.
18 J. B. Foresman and A. Frisch, *Exploring Chemistry with Electronic Structure Methods*, 2nd edn, Gaussian, Pittsburgh, 1993.
19 L. Zhu and W. L. Hase, *A general RRKM program (QCPE 644)*, Chemistry Department, University of Indiana, Bloomington, 1993.
20 S. G. Lias, J. E. Bartmess, J. F. Liebman, J. L. Holmes, R. D. Levin and W. G. Mallard, *J. Phys. Chem. Ref. Data*, 1988, **17**, 1.
21 S. G. Lias, in *NIST Standard Reference Database Number 69*, ed. P. J. Linstrom and W. G. Mallard, National Institute of Standards and Technology, Gaithersburg, MD, 2003, pp. http://webbook.nist.gov.
22 B. Ruscic, M. Schwrz and J. Berkowitz, *J. Chem. Phys.*, 1989, **91**, 6780.
23 B. Ruscic and M. Litorj, *Chem. Phys. Lett.*, 2000, **316**, 45.
24 W. v. Niessen, G. Bieri and L. Asbrink, *J. Electron Spectrosc. Relat. Phenom.*, 1980, **21**, 175.
25 K. Kimura, S. Katsumata, Y. Achiba, T. Yamazaki and S. Iwata, *Handbook of He-I photoelectron spectra of fundamental organic molecules*, Japan Scientific Societies Press, Tokyo, 1981.
26 P. C. Burgers, J. L. Holmes, F. P. Lossing, A. A. Mommers, F. R. Povel and J. K. Terlouw, *Can. J. Chem.*, 1982, **60**, 2246.
27 P. C. Burgers, A. A. Mommers and J. L. Holmes, *J. Am. Chem. Soc.*, 1983, **105**, 5976.
28 R. D. Levine and R. B. Bernstein, *Molecular Reaction Dynamics and Chemical Reactivity*, Oxford University Press, New York, 1987.
29 J. Liu, K. Song, W. L. Hase and S. L. Anderson, *J. Chem. Phys.*, 2003, **119**, 3040.
30 G. A. Fisk, J. D. McDonald and D. R. Herschbach, *Discuss. Faraday Soc.*, 1967, **44**, 228.
31 J. Troe, *Chem. Phys. Lett.*, 1985, **122**, 425.
32 J. Liu, B. Van Devener and S. L. Anderson, *J. Chem. Phys.*, 2005, **123**, 204313/1.
33 J. Liu, B. Van Devener and S. L. Anderson, *J. Chem. Phys.*, 2004, **121**, 11746.
34 J. Liu, B. Van Devener and S. L. Anderson, *J. Chem. Phys.*, 2002, **117**, 8292.
35 J. Liu, B. Uselman, B. Van Devener and S. L. Anderson, *J. Phys. Chem. A*, 2004, **108**, 9945.
36 M. S. Child, *Molecular Collision Theory*, Academic Press, London and New York, 1974.
37 R. D. Levine and R. B. Bernstein, *Molecular Reaction Dynamics and Chemical Reactivity*, Oxford University Press, New York, 1987.
38 J. Liu and S. L. Anderson, *J. Chem. Phys.*, 2004, **120**, 8528.

